Materials Transactions, Vol. 54, No. 4 (2013) pp. 618 to 625

EXPRESS REGULAR ARTICLE

Thermoelectric Characteristics of n-Type Bi_2Te_3 and p-Type Sb_2Te_3 Thin Films Prepared by Co-Evaporation and Annealing for Thermopile Sensor Applications

Jae-Hwan Kim*, Jung-Yeol Choi*, Jae-Man Bae*, Min-Young Kim* and Tae-Sung Oh

Department of Materials Science and Engineering, Hongik University, Seoul 121-791, Republic of Korea

A thermoelectric thin-film device consisting of n-type Bi_2Te_3 and p-type Sb_2Te_3 thin-film legs was prepared on a glass substrate by using co-evaporation and annealing process. The Seebeck coefficient and the power factor of the co-evaporated Bi_2Te_3 film were $-30\,\mu V/K$ and $0.7 \times 10^{-4}\,W/K^2{\cdot}m$, respectively, and became substantially improved to $-160\,\mu V/K$ and $16 \times 10^{-4}\,W/K^2{\cdot}m$ by annealing at 400°C for 20 min. While the Seebeck coefficient of the co-evaporated Sb_2Te_3 thin film was $72\,\mu V/K$, it increased significantly to 165–142 $\mu V/K$ by annealing at 200–400°C for 20 min. A maximum power factor of $25 \times 10^{-4}\,W/K^2{\cdot}m$ was achieved for the co-evaporated Sb_2Te_3 film by annealing at 400°C for 20 min. A thermopile sensor consisting of 10 pairs of n-type Bi_2Te_3 and p-type Sb_2Te_3 thin-film legs exhibited a sensitivity of 2.7 mV/K. [doi:10.2320/matertrans.M2013010]

(Received January 8, 2013; Accepted February 5, 2013; Published March 15, 2013)

Keywords: *thermoelectric sensor, thermopile, thin film, co-evaporation, annealing, bismuth telluride, antimony telluride*

1. Introduction

Recently, a large number of studies have focused on the development of micro thermal sensors which convert heat energies generated by various physical signals and chemical reactions into electrical signals.[1–6] Among various thermal sensors, thermopile sensors using Seebeck effect have several advantages such as high sensitivity, no offset and no need for biasing.[4–6] Thermopile sensors can be utilized to various applications such as infrared sensor, microcalorimeter, psychrometer, root-mean-square converter, electromagnetic field sensor, flow meter, vacuum sensor and accelerometer.[4–6]

A thermoelectric thin-film device can be classified as either an in-plane or cross-plane device according to the heat flow direction through the device.[2,4,5,7–9] Compared to the cross-plane type, in-plane devices have the advantages such as relatively high voltage generation at a small temperature difference, relatively short processing time with thin leg-thickness of a few micrometers and easy formation of electrical contact between p/n legs, which make in-plane devices more suitable for thermopile sensor applications.[4]

As the sensitivity of a thermoelectric thermopile is given by the ratio of the measured voltage to the incident radiation power,[10] thin films of large Seebeck coefficient are required to get a high sensitivity of a thermopile sensor. Various works have been performed to utilize thermoelectric thin films of Bi_2Te_3 and Sb_2Te_3 for thermopile devices.[4,5,7–9,11–14] Bi_2Te_3 and Sb_2Te_3 are narrow band-gap semiconductors with superior thermoelectric characteristics at room temperature and possess promising potential applications not only for thermopile sensors, but also for micro generators and micro coolers.[5,7,9]

While various processing techniques such as evaporation,[11,13–18] metal–organic chemical vapor deposition (MOCVD),[19] molecular beam epitaxy (MBE),[12,20,21] sputtering[21–25] and electrodeposition[4,5] can be used for thermoelectric thin-film fabrication, evaporation is attractive because it is less expensive process than MOCVD, MBE and sputtering.[17] Evaporation has also an advantage of easy formation of a thermopile device, compared to electrodeposition for which successive formation and removal of seedlayers for electrodeposition of p-type and n-type thin-film legs are required. However, evaporation of Bi_2Te_3 films using bulk single source causes severe compositional variation along the film thickness as well as difficulty of stoichiometry control due to the large difference in vapor pressures of Bi and Te.[11,16,17] Co-evaporation using Bi and Te dual sources can avoid such disadvantages of single source evaporation and achieve a stoichiometry control more easily.[11,16,17]

In this study, n-type Bi_2Te_3 and p-type Sb_2Te_3 films were co-evaporated and annealed to evaluate their thermoelectric properties for thermopile-sensor applications. A thermopile sensor was prepared on a glass substrate using n-type Bi_2Te_3 and p-type Sb_2Te_3 films, and its thermal sensing properties were characterized with applying a controlled temperature difference across the hot and cold ends of the thermopile sensor.

2. Experimental Procedure

N-type Bi_2Te_3 films of 1.5 μm-thickness were co-evaporated using two tungsten boats charged with Bi and Te granules, respectively. P-type Sb_2Te_3 films of 1.5 μm-thickness were also co-evaporated using two tungsten boats charged with Sb and Te granules. Electric power to each evaporation source was adjusted separately to control the thin-film composition. Before charging in a tungsten boat, Bi, Sb and Te granules were cleaned with 5% nitric acid, acetone, ethanol and deionized water to remove surface oxide layer. Glass substrates were heated to 150°C for Bi_2Te_3 co-evaporation and to 300°C for Sb_2Te_3 co-evaporation, respectively, by using halogen lamps installed in the evaporation chamber. Thickness of the Bi_2Te_3 and Sb_2Te_3 films was controlled using quartz-crystal thickness monitor and measured using alpha-step surface profiler after deposition. The Bi_2Te_3 and Sb_2Te_3 films were annealed in vacuum at 200–400°C for 20 min to improve their thermoelectric properties.

*Graduate Student, Hongik University

Compositions and crystalline phases of Bi_2Te_3 and Sb_2Te_3 films were analyzed by energy dispersive spectroscopy (EDS) and X-ray diffraction (XRD), respectively. The Seebeck coefficients (α) of Bi_2Te_3 and Sb_2Te_3 films were measured to the in-plane direction at room temperature by applying a temperature difference of 20°C across both ends of a film. The electrical resistivity (ρ) was measured using a four-point-probe. The power factor (P) of Bi_2Te_3 and Sb_2Te_3 films was evaluated using the relation of $P = \alpha^2/\rho$. Carrier concentration (n) and mobility (μ) of the Bi_2Te_3 and Sb_2Te_3 films were characterized using Hall measurements with AC magnetic field of 3000 gauss. Hall coefficient (R_H) is expressed as eq. (1) where e is the electric charge of electron, n is the carrier concentration, J_x is the current density applied to a specimen along x direction, E_y is the Hall field measured along y direction, and B_z is the magnetic field applied to z direction.

$$R_H = \frac{1}{en} = \frac{E_y}{J_x B_z} \tag{1}$$

After evaluating the Hall coefficient (R_H) of each film with measurement of the Hall field (E_y) by applying known J_x and B_z, we characterized the carrier concentration (n) of the Bi_2Te_3 and Sb_2Te_3 films using eq. (1). Electrical conductivity (σ) is expressed as eq. (2) where n and μ are carrier concentration and mobility, respectively. Substituting the conductivity (σ) measured by four-point probe and the carrier concentration (n) characterized by Hall measurement into eq. (2), we evaluated the carrier mobility (μ) of the Bi_2Te_3 and Sb_2Te_3 films.

$$\sigma = ne\mu \tag{2}$$

Figure 1 illustrates the fabrication process for a thermopile test specimen consisting of 10 pairs of n-type Bi_2Te_3 and p-type Sb_2Te_3 thin-film legs. With using a patterned metal mask, we co-evaporated 1.5-μm-thick Bi_2Te_3 thin-film legs of 9.2 mm-length and 1.0 mm-width and annealed at 400°C for 20 min. Then we formed 1.5-μm-thick Sb_2Te_3 thin-film legs using co-evaporation through a metal mask and successive annealing at 200°C for 20 min. The sensitivity of a thermopile sensor i.e., the slope of a Seebeck voltage-temperature difference curve, is directly related to the Seebeeck coefficients of Bi_2Te_3 and Sb_2Te_3 films. Thus, we chose the annealing temperatures of 400°C for Bi_2Te_3 thin-film legs and 200°C for Sb_2Te_3 thin-film legs, which were determined as the annealing conditions for a maximum Seebeck coefficient of each film. Then Al electrodes of 1 μm-thickness were sputtered to connect p-type and n-type thin-film legs. Electrode pads to measure a Seebeck voltage (ΔV) of the thermopile module were also formed by sputtering 1-μm-thick Al. We also sputtered 0.1 μm-thick Ti, 2 μm-thick Cu and 0.1 μm-thick Ti successively through a metal mask to form a Ti/Cu/Ti thin-film heater at the center region of the thermopile module.

A current was applied to the Ti/Cu/Ti thin-film heater to make a temperature difference (ΔT) across a hot end and a cold end of the thermopile sensor. Temperatures at the hot and cold ends of the thermopile were measured using thermocouples attached at each place. After reaching a steady-state temperature difference, an open-circuit voltage was measured as a Seebeck voltage (ΔV) of the thermopile sensor at a given temperature difference by using a digital multimeter.

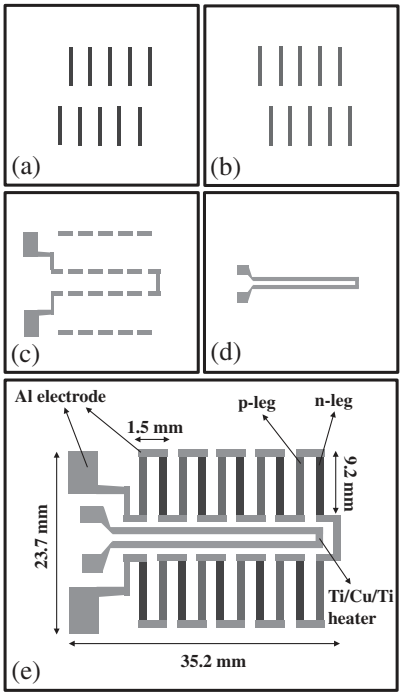

Fig. 1 Schematic illustration for the fabrication process of a thermopile-sensor test specimen: (a) co-evaporation and annealing of n-type Bi_2Te_3 thin-film legs, (b) co-evaporation and annealing of p-type Sb_2Te_3 thin-film legs, (c) sputtering of Al electrodes, (d) sputtering of a Ti/Cu/Ti thin-film heater and (e) overall configuration of the thermopile-sensor test specimen.

3. Results and Discussion

Table 1 lists the composition of the Bi_2Te_3 films, co-evaporated and annealed at each temperature, which was an average value of six measurements with about 5% deviation for each specimen. While the as-deposited Bi_2Te_3 film was Te-excess, the annealed films exhibited Bi-excess compositions. Such compositional variation would be caused by preferential vaporization of Te in the film during the annealing process due to the large difference between the vapor pressures of Te and Bi.[16] XRD patterns of co-evaporated and annealed Bi_2Te_3 films in Fig. 2 exhibited the polycrystalline structure of Bi_2Te_3 phase. Some of minor diffraction peaks were indexed as metallic Bi or Te. The crystalline nature of evaporated Bi_2Te_3 films seems to depend mainly upon a substrate temperature. It has been reported that Bi_2Te_3 films evaporated at 200–300°C were polycrystalline like our as-deposited film.[11,16,17] On the other hand, a Bi_2Te_3 film evaporated at room temperature was reported amorphous.[26] Figure 3 illustrates scanning electron micrographs of equiaxed grain structure of the as-deposited and the annealed Bi_2Te_3 films. The grain size of the Bi_2Te_3 films was calculated with the XRD data in Fig. 2 using Scherrer's relation[27] and listed in Table 1. The grain size of the as-deposited film was 24.5 nm and was enlarged up to 43.8 nm with increasing the annealing temperature up to 400°C.

Table 1 Composition and grain size of the Bi_2Te_3 film.

Annealing temperature, T/°C	Bi, /at%	Te, /at%	Grain size, /nm
As-deposited	30.2	69.8	24.5
200	42.8	57.2	28.8
300	45.5	54.5	36.9
400	46.2	53.8	43.8

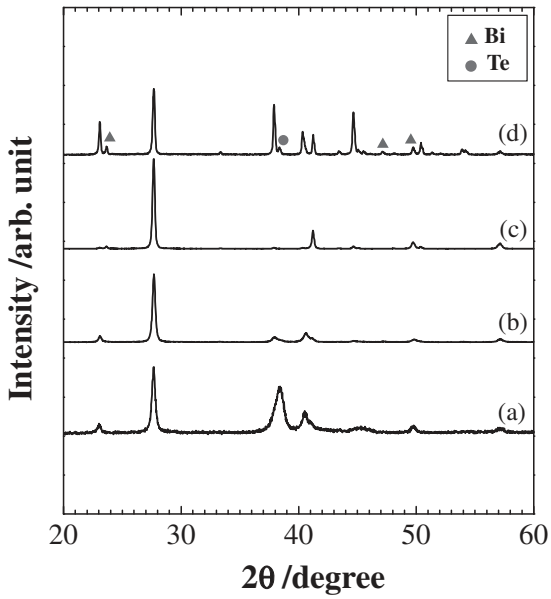

Fig. 2 X-ray diffraction patterns of the Bi_2Te_3 films (a) as-deposited and annealed at (b) 200°C, (c) 300°C and (d) 400°C. All the peaks except those indexed as Bi or Te were from the Bi_2Te_3 phase.

The Seebeck coefficient, electrical resistivity, carrier concentration and mobility of the Bi_2Te_3 films as a function of the annealing temperature were shown in Fig. 4. The annealed films as well as the as-deposited film have negative Seebeck coefficients due to their n-type conduction, which was confirmed by Hall-coefficient measurements. The Seebeck coefficient of the Bi_2Te_3 film, as shown in Fig. 4(a), was improved substantially from $-30\,\mu V/K$ up to $-160\,\mu V/K$ by the annealing treatment due to the decrease in the carrier concentration, as illustrated in Fig. 4(c). The Seebeck coefficient of $-160\,\mu V/K$ obtained for the Bi_2Te_3 film annealed at 400°C was lower than a reported value of $-248\,\mu V/K$ for the Bi_2Te_3 film co-evaporated at 270°C,[18] but comparable to -111 to $-195\,\mu V/K$ of the film co-evaporated at 240–300°C,[16] $-179\,\mu V/K$ of the film flash-evaporated and annealed at 250°C,[13] and $-130\,\mu V/K$ of the film co-sputtered and annealed at 400°C.[23]

For Bi_2Te_3 bulk single crystals, it has been reported that Te-excess composition is n-type due to Te_{Bi} antisite defects formed by incorporation of excess Te atoms into Bi sites and Bi-rich composition becomes p-type because of Bi_{Te} antisite defects generated by substitution of Bi atoms into Te vacancies.[28,29] As listed in Table 1, the composition of the as-deposited Bi_2Te_3 film was Te-rich, but became Bi-excess with the annealing treatment. However, the annealed films of Bi-excess composition as well as the Te-rich as-deposited film exhibited negative Seebeck coefficients, which is inconsistent with the conduction behavior reported for bulk Bi_2Te_3 single crystals.[29] The n-type conduction in a Bi-excess Bi_2Te_3 film has been also frequently reported by others for the films processed by co-sputtering[23] as well as co-evaporation.[16,17] Such discrepancy in major charge carriers between single crystals and thin films of Bi-excess Bi_2Te_3 might be attributed to the fact that more dislocations

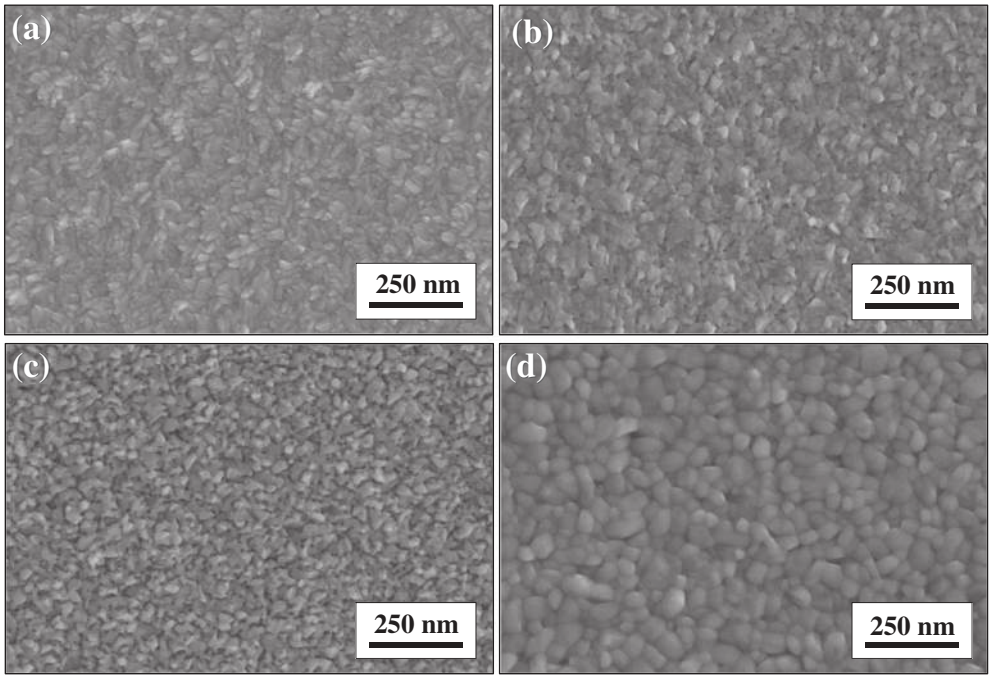

Fig. 3 Scanning electron micrographs of the Bi_2Te_3 films (a) as-deposited and annealed at (b) 200°C, (c) 300°C and (d) 400°C.

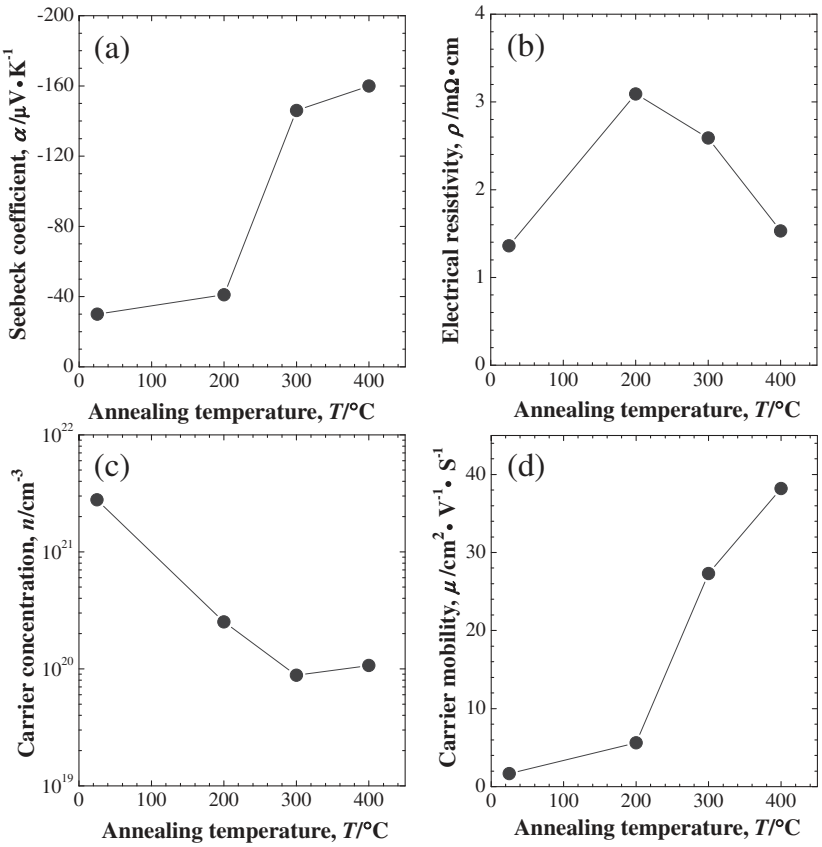

Fig. 4 (a) Seebeck coefficient, (b) electrical resistivity, (c) carrier concentration and (d) carrier mobility of the Bi_2Te_3 film as a function of the annealing temperature.

are generated and more oxygen can be incorporated in the lattice during thin-film processing.[20,28] As dislocation and oxygen in the Bi_2Te_3 lattice act as donors,[28,30,31] the p–n transition in a Bi_2Te_3 thin film would be shifted from the exact stoichiometry to Bi-rich composition regime.

In n-type Bi_2Te_3, the major charge carriers are electrons generated by Te_{Bi} antisite defects.[28–31] Thus, the decrease in the Te content of the Bi_2Te_3 film by the annealing treatment, as listed in Table 1, reduced the number of Te_{Bi} antisite defects, resulting in the carrier-concentration decrease from 2.8×10^{21} to $1.1 \times 10^{20}\,cm^{-3}$ by annealing at 400°C, as shown in Fig. 4(c). Such decrease in the carrier concentration with annealing process was also reported for n-type Bi_2Te_3 films fabricated by co-sputtering.[23] As illustrated in Fig. 4(d), the carrier mobility of the co-evaporated Bi_2Te_3 film increased from $1.7\,cm^2/V{\cdot}s$ up to $38.2\,cm^2/V{\cdot}s$ by the annealing treatment. Comparison of the carrier-mobility variation in Fig. 4(d) with the grain size listed in Table 1 implies that the grain growth of the film could be the main cause for mobility improvement by the annealing process. Reduction of point defects such as antisite defects would also partly attribute to the mobility enhancement. As shown in Fig. 4(b), the electrical resistivity increased from 1.4 to $3.1\,m\Omega{\cdot}cm$ by annealing at 200°C and then decreased to $1.5\,m\Omega{\cdot}cm$ by increasing annealing temperature further up to 400°C.

Table 1 lists the composition of the Sb_2Te_3 films, co-evaporated and annealed at each temperature, which was an average value of six measurements with about 5% deviation for each specimen. The as-deposited Sb_2Te_3 film exhibited a Sb-rich composition. Interestingly, the compositional change of the Sb_2Te_3 film by the annealing treatment was almost negligible, which was different from the substantial decrease in the Te content of the Bi_2Te_3 film by the annealing treatment (Table 1). Such difference in the compositional change of the Sb_2Te_3 film with the Bi_2Te_3 film may be related to re-evaporation of Te in each film during the annealing process. Goncalves *et al.*[16] reported that while severe re-evaporation of Te occurred from the film during co-evaporation of a Bi_2Te_3 film, it was negligible during the co-evaporation of a Sb_2Te_3 film. Also, we co-evaporated the Sb_2Te_3 film at 300°C higher than 150°C for the Bi_2Te_3 film, which might partly contribute to minimize re-evaporation of Te and composition change by the annealing process.

XRD patterns in Fig. 5 reveal the polycrystalline structure of Sb_2Te_3 phase with minor diffraction peaks of metallic Sb and Te for the as-deposited film as well as the annealed films. Like the Bi_2Te_3 film, the crystalline nature of evaporated Sb_2Te_3 films depends upon a substrate temperature. While Sb_2Te_3 films co-evaporated at 200–300°C were crystalline,[11,16] films prepared at room temperature by evaporation of single Sb_2Te_3 alloy source or dual sources of elemental Sb and Te turned out to be amorphous.[15,32] Sb_2Te_3 films grown by MBE at 200°C or prepared by MOCVD at 450°C were also crystalline.[12,19] Figure 6 illustrates the scanning electron micrographs of the as-deposited and the annealed Sb_2Te_3 films. While it is not clear that the grain size was changed by the annealing treatment at 200–300°C, the grain size was

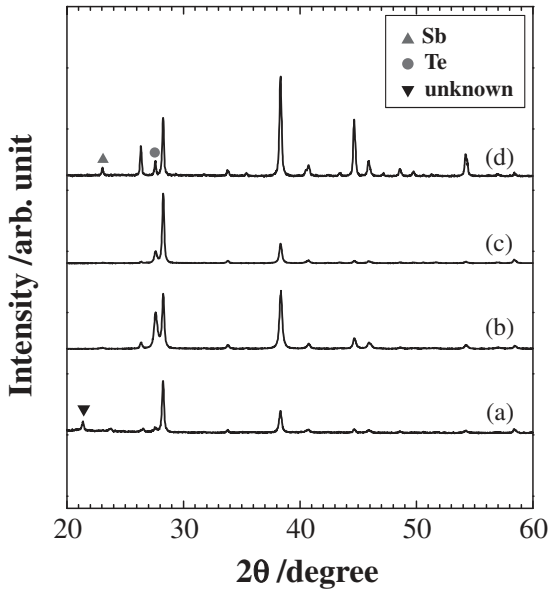

Fig. 5 X-ray diffraction patterns of the Sb_2Te_3 films (a) as-deposited and annealed at (b) 200°C, (c) 300°C and (d) 400°C. All the peaks except those indexed as Sb, Te or unknown were from the Sb_2Te_3 phase.

obviously enlarged by annealing at 400°C. The grain size of the Sb_2Te_3 films was calculated with the XRD data in Fig. 5 using Scherrer's relation[27] and listed in Table 2. The grain size of the as-deposited film was 37.8 nm and did not increase with annealing at 200 and 300°C which were lower than or equal to the co-evaporation temperature of 300°C. On the other hand, the grain size was substantially enlarged to 50.5 nm by annealing at 400°C.

Thermoelectric properties of the Sb_2Te_3 films were illustrated in Fig. 7 as a function of the annealing temperature. The annealed films as well as the as-deposited film have positive Seebeck coefficients due to their p-type

Table 2 Composition and grain size of the Sb_2Te_3 film.

Annealing temperature, T/°C	Sb, /at%	Te, /at%	Grain size, /nm
As-deposited	43.8	56.2	37.8
200	46.3	53.7	35.3
300	40.9	59.1	38.7
400	44.8	55.2	50.5

conduction, which was confirmed by Hall-coefficient measurements. The Seebeck coefficient of the as-deposited Sb_2Te_3 film was 72 μV/K and was improved by annealing treatment. A maximum Seebeck coefficient of 165 μV/K was obtained with annealing at 200°C. The Seebeck coefficients of 165–142 μV/K, obtained for the Sb_2Te_3 films annealed at 200–400°C, were comparable to or higher than values of 111–153 μV/K reported for the Sb_2Te_3 films co-evaporated at temperatures ranging from 240 to 300°C,[16] 65–115 μV/K of the film prepared by MOCVD[19] and 80–120 μV/K of the film grown by MBE.[12]

As shown in Fig. 7(c), the carrier concentration of the Sb_2Te_3 film decreased from 4.4×10^{20} to 6.6×10^{19} cm^{-3} with annealing at temperatures up to 400°C. As the composition of the Sb_2Te_3 film was not changed with the annealing treatment (Table 2), the decrease in the carrier concentration with increasing the annealing temperature could be attributed to the reduction of point defects such as Sb_{Te} antisite defects and Sb vacancies acting as acceptors in the Sb_2Te_3 lattice.[12,25,33] Decrease in the carrier concentration with increasing the annealing temperature was also reported for the Sb_2Te_3 film fabricated by radio frequency magnetron sputtering.[22] As illustrated in Fig. 7(d), the carrier mobility of the co-evaporated Sb_2Te_3 film increased by the annealing treatment, which could be partly due to the reduction of point

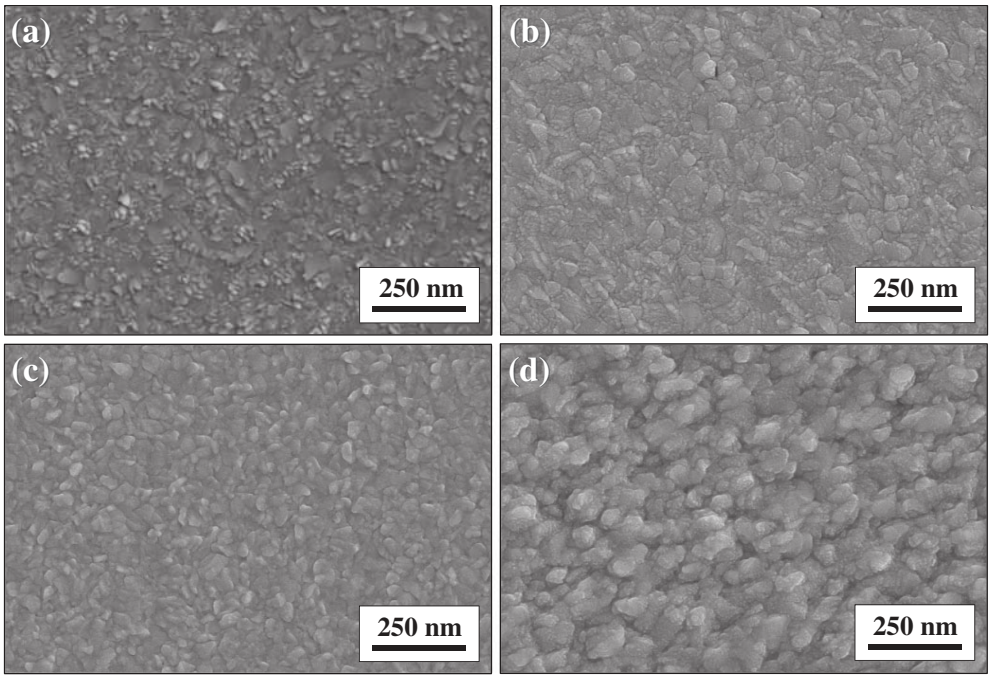

Fig. 6 Scanning electron micrographs of the Sb_2Te_3 films (a) as-deposited and annealed at (b) 200°C, (c) 300°C and (d) 400°C.

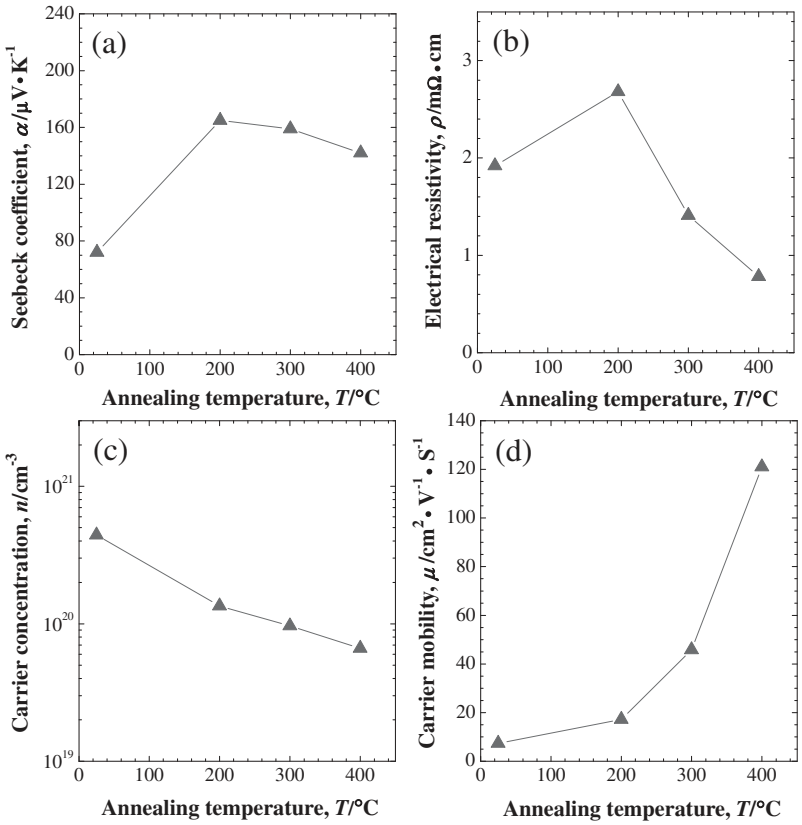

Fig. 7 (a) Seebeck coefficient, (b) electrical resistivity, (c) carrier concentration and (d) carrier mobility of the Sb_2Te_3 film as a function of the annealing temperature.

defects and partly due to the grain growth of the film. Comparison of the carrier-mobility variation with the grain size listed in Table 2 implies that while the main cause for the mobility improvement by annealing process at 200–300°C was the reduction of point defects, the substantial increase in the carrier mobility by annealing at 400°C could be attributed both to the reduction of point defects and to the grain growth. As shown in Fig. 7(b), the electrical resistivity of the Sb_2Te_3 film increased from 1.9 to 2.7 mΩ·cm by annealing at 200°C and then decreased to 0.8 mΩ·cm by increasing the annealing temperature further to 400°C.

Figure 8 shows the power factor of the Bi_2Te_3 film and the Sb_2Te_3 film as a function of the annealing temperature. The power factor of the Bi_2Te_3 film was improved to 16×10^{-4} W/K^2·m by annealing at 400°C, which is lower than 48.7×10^{-4} W/K^2·m reported for the Bi_2Te_3 film co-evaporated on a polyimide substrate,[18] but comparable to or higher than 15.7×10^{-4} and 9×10^{-4} W/K^2·m of the films processed by co-sputtering,[8,13,23] 5.5×10^{-4} W/K^2·m of the electrodoposited film[5] and 2.9×10^{-4} W/K^2·m of the Bi_2Te_3 film grown by co-evaporation.[9] The power factor of the Sb_2Te_3 film was improved with increasing the annealing temperature and reached to 25×10^{-4} W/K^2·m by annealing at 400°C, which is lower than 81×10^{-4} W/K^2·m reported for the electrodeposited Sb_2Te_3 film,[5] but comparable to or higher than 28×10^{-4} W/K^2·m of the film prepared by co-evaporation,[18] 22×10^{-4} W/K^2·m of the film grown by ion beam sputtering,[25] 8×10^{-4} W/K^2·m of the films processed by co-evaporation[16] and 4×10^{-4} W/K^2·m of the film fabricated by ion beam sputtering.[24]

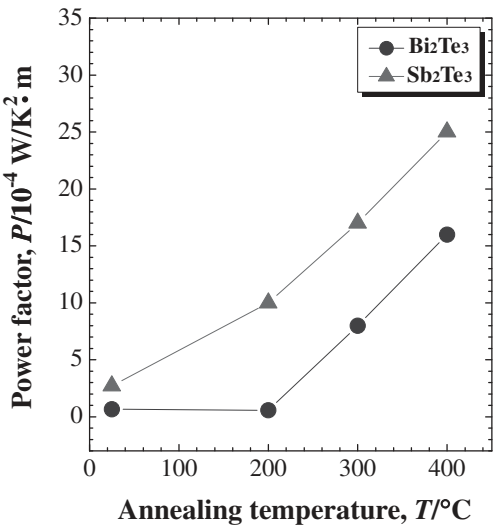

Fig. 8 Power factor of the Bi_2Te_3 and the Sb_2Te_3 films as a function of the annealing temperature.

Figure 9 illustrates an optical micrograph of a thermopile-sensor test-specimen consisting of 10 pairs of n-type Bi_2Te_3 and p-type Sb_2Te_3 thin-film legs on a glass substrate. A Ti/Cu/Ti thin film heater was formed to make a temperature difference across the hot and cold ends of the thermopile module. Figure 10 reveals the linear dependence of the Seebeck voltage generated by the thermopile sensor upon the temperature difference formed across the hot and cold ends of the sensor. The thermopile sensor exhibited a sensitivity,

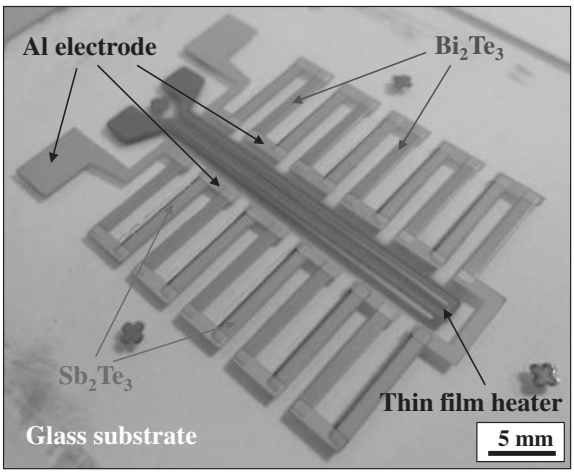

Fig. 9 Optical micrograph of a thermopile-sensor test-specimen consisting of a thermopile module and a thin-film heater.

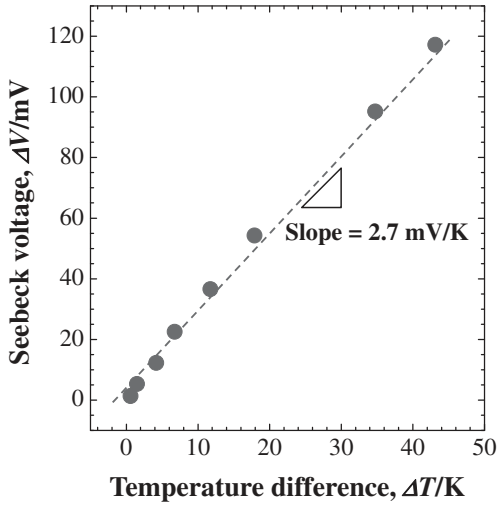

Fig. 10 Seebeck voltage (ΔV) of the thermopile sensor as a function of the temperature difference (ΔT).

i.e., the slope of the Seebeck voltage-temperature difference curve, of 2.7 mV/K, which was much larger than 0.19 mV/K measured for a thermoelectric sensor prepared with single pair of silicon-on-insulator structure and 1.2 mV/K predicted for a mini-device consisting of 4 pairs of evaporated Bi_2Te_3 and Sb_2Te_3 thin-film legs.[11,34] The sensitivity of our thermopile sensor was comparable to 2.7 mV/K reported for a thermoelectric generator consisting of 7 pairs of Bi_2Te_3 and Sb_2Te_3 thin films processed by flush evaporation and hydrogen annealing.[13]

As shown in Figs. 4(a) and 7(a), the n-type Bi_2Te_3 film annealed at 400°C and the p-type Sb_2Te_3 film annealed at 200°C have the Seebeck coefficients of −160 and 165 μV/K, respectively. Thus, the thermopile module consisting of 10 pairs of the n-type Bi_2Te_3 and the p-type Sb_2Te_3 thin-film legs would give an ideal sensitivity of 3.3 mV/K. Considering that the Bi_2Te_3 and the Sb_2Te_3 thin-film legs were much thinner than the glass substrate, the difference between the actual sensitivity of 2.7 mV/K and the ideal sensitivity of 3.3 mV/K was not significant. For the in-plane thermopile configuration where thin-film legs are fabricated parallel to a thick substrate as shown in Fig. 9, a temperature difference across the hot and cold ends causes heat flow through thin-film legs and a substrate simultaneously. The thinner thin-films legs are, the less heat flows through thin-film legs. Thickening the Bi_2Te_3 and Sb_2Te_3 thin-film legs would enhance the heat flow through thin-film legs and increase the actual sensitivity of the thermopile sensor close to the ideal sensitivity expected with the Seebeck coefficients of the films.

4. Conclusion

While the as-deposited Bi_2Te_3 film was Te-excess, the annealed films exhibited Bi-excess compositions due to preferential vaporization of Te during the annealing process. However, the annealed Bi_2Te_3 films of Bi-excess composition as well as the Te-rich as-deposited film exhibited negative Seebeck coefficients, which is inconsistent with the p-type conduction of Bi-excess bulk Bi_2Te_3 single crystal. Such discrepancy in major charge carrier type between single crystals and thin films of Bi-excess Bi_2Te_3 might be attributed to the fact that more dislocations and oxygen acting as donors are contained in a thin film due to the processing nature, shifting the p-n transition in a Bi_2Te_3 thin film from the exact stoichiometry to Bi-rich composition regime. The n-type Bi_2Te_3 film co-evaporated and annealed at 400°C for 20 min exhibited a Seebeck coefficient of −160 μV/K and a power factor of 16×10^{-4} W/K^2·m. Seebeck coefficients of 165–142 μV/K were obtained by annealing the co-evaporated Sb_2Te_3 at 200–400°C for 20 min and a maximum power factor of 25×10^{-4} W/K^2·m was achieved for the Sb_2Te_3 film annealed at 400°C. A thermopile sensor composing of 10 pairs of n-type Bi_2Te_3 and p-type Sb_2Te_3 thin-film legs exhibited a sensitivity of 2.7 mV/K, which was close to the ideal sensitivity of 3.3 mV/K estimated using the Seebeck coefficients of the Bi_2Te_3 and the Sb_2Te_3 films. Thickening the Bi_2Te_3 and the Sb_2Te_3 thin-film legs would further improve the sensitivity of the thermopile sensor.

Acknowledgement

This work was supported by the Basic Science Research Program of the National Research Foundation of Korea (Project No.: 2010-0009642).

REFERENCES

1) J. P. Carmo, J. F. Ribeiro, M. F. Goncalves and J. H. Correia: J. Micromech. Microeng. **20** (2010) 1–8.
2) W. Glatz, E. Schwyter, L. Durrer and C. Hierold: J. Microelectromech. Syst. **18** (2009) 763–772.
3) Z. Wang, B. Leonov, P. Fiorini and C. V. Hoof: Sens. Actuators A **156** (2009) 95–102.
4) M. Y. Kim and T. S. Oh: Mater. Trans. **51** (2010) 1909–1913.
5) M. Y. Kim and T. S. Oh: Mater. Trans. **53** (2012) 2160–2165.
6) S. Herwaarden: Proc. 16th Int. Conf. on Thermoelectrics, (International Society of Thermoelectrics, 1997) pp. 47–55.
7) G. J. Snyder, J. R. Lim, C.-K. Huang and J.-P. Fleurial: Nature Mater. **2** (2003) 528–531.
8) H. Bottner, J. Nurnus, A. Gavrikov, G. Kuhner, M. Jagle, C. Kunzel, D. Eberhard, G. Plescher, A. Schubert and K.-H. Schlereth: J. Microelectromech. Syst. **13** (2004) 414–420.

9) L. W. da Silva, M. Kaviany, A. DeHennis and J. S. Dyck: Proc. 22nd Int. Conf. on Thermoelectrics, (International Society of Thermoelectrics, 2003) pp. 665–668.
10) M. Müller, W. Budde, G. Gottfried, A. Hüber, R. Jähne and H. Kück: Sens. Actuators A **54** (1996) 601–605.
11) L. M. Goncalves, C. Couto, P. Alpuim, D. M. Rowe and J. H. Correia: Sens. Actuators A **130–131** (2006) 346–351.
12) Y. Kim, A. DiVenere, G. K. L. Wong, J. B. Ketterson, S. Cho and J. R. Meyer: J. Appl. Phys. **91** (2002) 715–718.
13) M. Takashiri, T. Shirakawa, K. Miyazaki and H. Tsukamoto: Sens. Actuators A **138** (2007) 329–334.
14) L. M. Goncalves, J. G. Rocha, C. Couto, P. Alpuim, G. Min, D. M. Rowe and J. H. Correia: J. Micromech. Microeng. **17** (2007) S168–S173.
15) B. Lv, S. Hu, W. Li, X. Di, L. Feng, J. Zhang, L. Wu, Y. Cai, B. Li and Z. Lei: Int. J. Photonenergy **2010** (2010) Article ID 476589.
16) L. M. Goncalves, P. Alpuim, G. Min, D. M. Rowe, C. Couto and J. H. Correia: Vacuum **82** (2008) 1499–1502.
17) H. Zou, D. M. Rowe and G. Min: J. Cryst. Growth **222** (2001) 82–87.
18) J. P. Carmo, L. M. Goncalves and J. H. Correia: Electron. Lett. **45** (2009) 803–804.
19) A. Giani, A. Boulouz, F. Pascal-Delannoy, A. Foucaran, A. Boyer, B. Aboulfarah and A. Mzerd: J. Mater. Sci. Lett. **18** (1999) 541–543.
20) N. Peranio, O. Eibl and J. Nurnus: J. Appl. Phys. **100** (2006) 114306.
21) N. Peranio, M. Winkler, Z. Aabdin, J. Konig, H. Bottner and O. Eibl: Phys. Status Solidi A **209** (2012) 289–293.
22) B. Fang, Z. Zeng, X. Yan and Z. Hu: J. Mater. Sci: Mater. Electron. (2012) doi:10.1007/s10854-012-0888-1.
23) D. H. Kim and G. H. Lee: Mater. Sci. Eng. B **131** (2006) 106–110.
24) P. Fan, Z. H. Zheng, G. X. Liang, X. M. Cai and D. P. Zhang: Chin. Phys. Lett. **27** (2010) 087201.
25) P. Fan, Z. H. Zheng, G. X. Liang, D. P. Zhang and X. M. Cai: J. Alloy. Compd. **505** (2010) 278–280.
26) J. Dheepa, R. Sathyamoorthy and A. Subbarayan: J. Cryst. Growth **274** (2005) 100–105.
27) B. D. Cullity: *Elements of X-ray Diffraction*, (Addisson Wesley, Reading, 1982) p. 102.
28) A. Hashibon and C. Elsasser: Phys. Rev. B **84** (2011) 144117.
29) S. W. Jun, K. Y. Lee and T. S. Oh: J. Korean Phys. Soc. **48** (2006) 1708–1712.
30) J. M. Schultz, J. P. McHugh and W. A. Tiller: J. Appl. Phys. **33** (1962) 2443–2450.
31) D. M. Gel'fgat and Z. M. Dashevskii: Inorg. Mater. **19** (1984) 1172–1173.
32) P. Arun, P. Tyagi, A. G. Vedeshwar and V. K. Paliwal: Physica B **307** (2001) 105–110.
33) Y. Jiang, Y. Y. Sun, M. Chen, Y. Wang, Z. Li, C. Song, K. He, L. Wang, X. Chen, Q. K. Xue, X. Ma and S. B. Zhang: Phys. Rev. Lett. **108** (2012) 066809.
34) W. H. Lee, Y. T. Lee, H. Takao, K. Sawada and M. Ishida: Jpn. J. Appl. Phys. **46** (2007) 7232–7236.